VIBRATION SIGNATURE ANALYSIS OF ROLLING BEARINGS UNDER RADIAL CLEARANCE AND RACEWAY FAULTS

[1]Hari,[2]Naresh,[3]Swarna Latha

[123]Students

Department of Mechanical Engineering

ABSTRACT:

Rolling bearings are critical components in rotating machinery, and their degradation often leads to performance loss, unexpected failures, and increased maintenance costs. This study focuses on the vibration signature analysis of rolling bearings considering two key fault parameters: radial clearance and outer raceway defects. Variations in radial clearance and surface damage on the raceway significantly alter the system's dynamic behavior, producing distinguishable vibration patterns that can be analyzed for early fault detection. Through a combination of numerical modeling, finite element simulation, and experimental vibration analysis, the study identifies characteristic frequency components, amplitude shifts, and modulation effects associated with these defects. The results indicate that increasing radial clearance amplifies the vibration response, while raceway defects introduce periodic impacts that are observable in both the time and frequency domains. This research supports the development of condition-based monitoring systems for predictive maintenance in industrial applications.

I.INTRODUCTION:

Rotating machinery in industrial applications relies heavily on the performance of rolling element bearings, which are subjected to varying loads, speeds, and environmental conditions. Over time, bearings may develop faults such as increased radial clearance, surface wear, or raceway pitting, which can compromise the operational stability of the entire system. Among these, radial clearance variation and outer raceway defects are common yet critical issues that influence the dynamic behavior of the rotor–bearing system.

Vibration analysis is a widely adopted technique in the field of condition monitoring and fault diagnosis. Each type of defect in a bearing produces a unique vibration signature, often observable in time-domain waveforms or frequency spectra. However, when multiple faults like clearance changes and raceway damage coexist, the complexity of the vibration response increases, making detection and interpretation more challenging.

This study aims to investigate how radial clearance levels and outer raceway defects affect the vibration characteristics of rolling bearings supporting a rotor system. By performing detailed signal analysis, the research identifies fault-specific indicators that can enhance fault detection accuracy and reduce downtime. The study combines both experimental testing and simulation-based modeling to ensure accurate characterization of vibration responses. This knowledge is essential for advancing predictive maintenance strategies and improving the reliability of mechanical systems

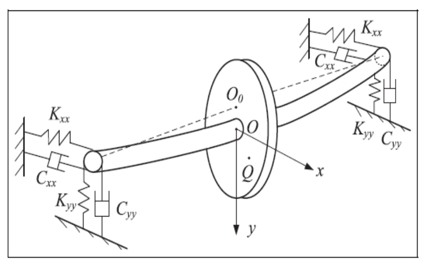

Figure 1. Dynamical model of bearing rotor system.

excitation, and calculated the vibration response of time domain and the frequency domain characteristics of the rotor under the time-varying bearing stiffness. Liu and Zhang17 deduced the time-varying stiffness of rolling bearings under different combined load sets by the implicating function derivation.

The vibration and shock of the bearing rotor system is caused by the time-varying characteristic of rolling bearing stiffness, which aggravates the generation of small defects on the raceway. Cheng et al.18 established a quasi-static analysis model of rolling bearing with local defects by introducing the local contour functions such as the depth and circumferential variation of local into the analysis model. Petersen et al.19 established a contact stiffness model of bearing related to the defect size based on the internal load distribution of rolling bearings with defects in the outer ring. Cui et al.20 simulated the vibration response signals of rolling bear- ings under different fault sizes by introducing the outer ring defect size parameters into the dynamic model. Jiang et al.21 improved the dynamic model with three- dimensional geometric defect regions by extending the geometric parameters of the outer raceway defect regions. Singh et al.22 solved the bearing FEM model with outer raceway defect by LS-DYNA, and analyzed the simulation results. Zhao et al.23 researched the effects of defect size, position, and number on bearing dynamic behaviors are investigated with the aid of phase trajectories, shaft center orbits, FFT spectra, etc. Tang et al.24 analyzed the load of rolling elements pass- ing through the defect area under different conditions based on Gupta model. Ma et al.25 added the three dif- ferent types of bearing defects into the defect model considering the force transfer between the vehicle and the bearing. Lu et al.26 proposed the defect modeling algorithm of inner raceway, outer raceway and rolling element, and obtained the theoretical rolling track when the rolling element passes through the defect position. These studies only consider the defects of roll- ing bearings, but don't consider the time-varying char- acteristics of bearing stiffness.

The dynamic model of rolling bearing rotor system considering the radial clearance and outer raceway defect is established for the spindle bearings of machine tool in this paper. The time-varying stiffness of bearing is fitted, and the vibration response of rolling bearing rotor system is analyzed. The fault characteristic fre- quency of rolling bearing identified by the vibration response is compared with the experiment results.

Dynamical modeling of rolling bearing rotor system

Dynamical model of rotor system

For the rolling bearing rotor system, the rotor is sup- ported by two identical rolling bearings at both ends, and the external load is applied at the middle position. The bearing can be simplified as an isotropic spring- damp system assuming that the bearing is supported rigidly.27 The stiffness and damping coefficients in the horizontal direction are kxx and cxx respectively, and in the vertical direction are kyy and cyy respectively.

The dynamical model of the bearing rotor system is shown in Figure 1. O0 is the center of the static balance of the rotor. When the rotor rotates, the unbalanced force causes the axis to deviate from the static balance position. At this time, the center of rotor is O, which is the original point of coordinate system xOy.

According to the principle of force balance, the dif- ferential equations of motion of rolling bearing rotor system are:

$$\begin{cases} M \cdot \ddot{x} + C \cdot \dot{x} + K_x \cdot x = F_0 \cdot \sin(\omega \cdot t) \\ M \cdot \ddot{y} + C \cdot \dot{y} + K_y \cdot y = F + F_0 \cdot \cos(\omega \cdot t) + M \cdot g \end{cases} \quad (1)$$

Where M is the mass of bearing-rotor system. C is the supporting damping coefficient of bearing-rotor system, which is the contact damping of rolling bear- ing.28 Kx, Ky are the equivalent stiffness of the rolling bearing rotor system in the horizontal and vertical directions, Kx = k kxx/(k + kxx), Ky = k kyy/(k + kyy), k is the rotor bending stiffness, k = 12pER4 /L3. E is the elastic modulus. R is the journal radius. L is the dis- tance between the center of two bearings. v is the angu- lar speed of the rotor. F0 is the centrifugal force caused by the unbalanced mass of the rotor. g is the gravita- tional acceleration. F is the external exciting force.

Rolling bearing stiffness model with outer raceway defects

Defect model on outer raceway. It is supposed that there is a rectangular notch on the outer raceway ring,29 the defect depth is Hb, the defect length is Lb, the corre- sponding wrap angle is ub, the diameter of the rolling

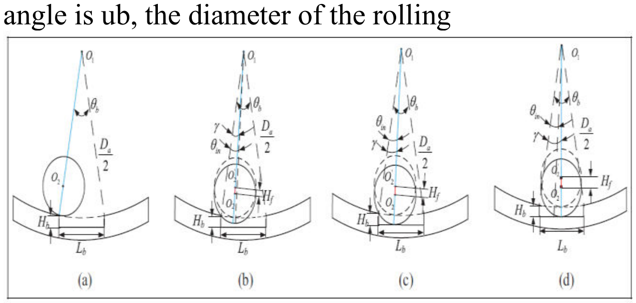

Figure 2. Additional displacement of rolling elements passing through defect of outer raceway: (a) $\gamma = 0$, (b) $0 < \gamma < \theta_{in}$, (c) $\gamma = \theta_{in}$, and (d) $\theta_{in} < \gamma < \theta_b - \theta_{in}$.

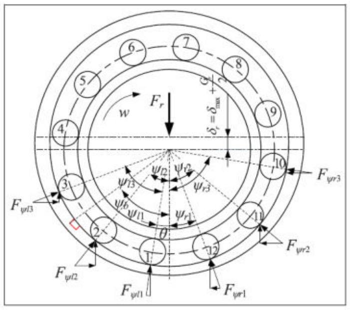

Figure 3. Force analysis of rolling bearing with radial clearance.

element is Dw, and the diameter of the outer raceway of the bearing is Da. Form the rolling element enters the defect to leaves the defect, Hf is the additional displacement of the rolling element, and g is the angle between the center of rolling element and the starting position of the defect. For the large outer raceway defect (Dw\Lb), when the rolling element begin to enter the outer raceway defect (g=0), the additional displacement is 0 (as shown in Figure 2(a)). When the rolling element passes through the bottom of outer raceway defect (ub2uin ł g ł ub), the additional displacement is the maximum value at this time, which is equal to the defect depth of the outer raceway (as shown in Figure 2(d)). When the rolling element is entering or leaving the defect (0\g\uin or ub2uin\g\ub), it only contacts with one side of the defect (as shown in Figure 2(b)). In order to analyze the additional displacement of the rolling element during the rolling element passage through the outer raceway defect, the change of the additional displacement is simplified as the linear change, and the defect is assumed to be a smooth surface. The wrap angle between the starting point of the outer ring defect area and the point of the maximum additional displacement uin is proposed to calculate the additional displacement Hf, which can be expressed as follows:

$$\theta_{in} \approx \arcsin\left(\sqrt{\left(\frac{D_w}{2}\right)^2 - \left(\frac{D_w}{2} - H_b\right)^2} \Big/ \frac{D_a}{2}\right) \quad (2)$$

When the rolling element passes through the outer raceway defect position, the additional displacement of the rolling element Hf can be expressed as:

$$H_f = \begin{cases} \dfrac{H_b \gamma}{\theta_{in}}, & 0 < \gamma < \theta_{in} \\ H_b, & \theta_{in} \leqslant \gamma \leqslant \theta_b - \theta_{in} \\ \dfrac{H_b}{\theta_{in}}(\theta_b - \gamma), & \theta_b - \theta_{in} < \gamma < \theta_b \\ 0, & another \end{cases} \quad (3)$$

The similar method can be used to analyze the small outer raceway defect (Dw . Lb), which is not be described because of the length of this paper.

Stiffness model of rolling bearing. The defects could exist anywhere in the outer raceway, the outer raceway can be divided into loading area and non-loading area accord- ing to the load distribution (as shown in Figure 3). When the defect of the outer raceway is in the non-loading area, there is almost no impact on the dynamic charac- teristics of the bearing because the rolling element does not contact with the track of rolling bearing. Therefore, the defect of the outer raceway in the loading area is analyzed.

The force analysis of rolling bearing with radial clearance is shown in Figure 3. u is the rotation posi- tion angle of the rolling element. v is the angular velo- city of the rolling bearing. cb is the angle between the is the angle between the left rolling elements and the bearing axis in the vertical direction. cri is the angle

between the right rolling elements and the bearing axis in the vertical direction. When the rolling element passes through the defect of the rolling bearing without radial clearance, the additional displacement will result in the change of load distribution and local elastic deformation. The elastic deformation of the rolling element along the Hertz contact normal line can be expressed as:

$$\delta_{\psi_b} = \delta_{\max} \cos \psi_b - H_f \quad (4)$$

Where dcb is the elastic deformation of the rolling ele- ment at the defect, dmax is the maximum elastic defor- mation of the elastomer. The load of the rolling element at the defect Fcb is:

$$F_{\psi_b} = F_{\max}\left(\frac{\delta_{\psi_b}}{\delta_{\max}}\right)^{1.5} = F_{\max}\left(\cos \psi_b - \frac{H_f}{\delta_{\max}}\right)^{1.5} \quad (5)$$

Where Fmax is the maximum load of the rolling element According to the principle of force balance, the

radial load of rolling bearing should be equal to the resultant force of each rolling element in the vertical
direction:

$$F_r = F_{\max}\left[\sum_{i=1}^{n}\cos^{2.5}(\psi_i+\omega t)+\left(\cos\psi_b-\frac{H_f}{\delta_{\max}}\right)^{1.5}\cos\psi_b\right] \quad (6)$$

Where Fr is the radial external load of the rolling bearing.
The maximum load of the rolling element can be expressed as:

$$F_{\max} = \frac{F_r}{\left[\sum_{i=1}^{n}\cos^{2.5}(\psi_i+\omega t)+\left(\cos\psi_b-\frac{H_f}{\delta_{\max}}\right)^{1.5}\cos\psi_b\right]} \quad (7)$$

The load distribution of each rolling element of rolling bearing without radial clearance can be expressed as30:

$$F_{\psi_i} = \frac{F_r\cos^{1.5}\psi_i}{\left[\sum_{i=1}^{n}\cos^{2.5}(\psi_i+\omega t)+\left(\cos\psi_b-\frac{H_f}{\delta_{\max}}\right)^{1.5}\cos\psi_b\right]} \quad (8)$$

When the rolling element passes through the defect of bearing with radial clearance, the elastic deformation of the rolling element along the Hertz contact normal line can be expressed as:

$$\delta_{\psi_b} = \left(\delta_{\max}+\frac{G_r}{2}\right)\cos\psi_b-\frac{G_r}{2}-H_f \quad (9)$$

Where Gr is the radial clearance of bearing. The load of the rolling element at the defect can be obtained from the derivation of the above formula for the load distribution on each rolling element of the rolling bearing without radial clearance, which can be expressed as:

$$F_{\psi_b} = F_{\max}\left(\frac{\delta_{\psi_b}}{\delta_{\max}}\right)^{1.5} = F_{\max}\left(\frac{(\delta_{\max}+G_r/2)\cos\psi_b-G_r/2-H_f}{\delta_{\max}}\right)^{1.5} \quad (10)$$

The load distribution coefficient T is proposed to simplify the maximum load Fmax of rolling element of rolling bearing with radial clearance. Define T=(12Gr/(2dmax + Gr))/2, so the Fcb can be expressed as:

$$F_{\psi_b} = F_{\max}\left(\frac{\cos\psi_b}{2T}-\frac{G_r/2+H_f}{\delta_{\max}}\right)^{1.5} \quad (11)$$

The iteration process of solving Fmax is shown in Figure 4. Therefore, the maximum load of the rolling bearing with the radial clearance Fmax at the nth iteration can be expressed:

$$F^n_{\max} = \frac{F_r}{\left(\sum_{i=1}^{m}\left(\frac{\delta^n_r\cos\psi_i-G_r/2}{\delta^n_{\max}}\right)^{1.5}\cos\psi_i+\left(\frac{\delta^n_r\cos\psi_b-G_r/2-H_f}{\delta^n_{\max}}\right)^{1.5}\cos\psi_b\right)}$$

$$= \frac{\sum_{i=1}^{m}F_{\psi_i}\cos\psi_i+F_{\psi_b}\cos\psi_b}{\left(\sum_{i=1}^{m}\left(\frac{\delta^n_r\cos\psi_i-G_r/2}{\delta^n_{\max}}\right)^{1.5}\cos\psi_i+\left(\frac{\delta^n_r\cos\psi_b-G_r/2-H_f}{\delta^n_{\max}}\right)^{1.5}\cos\psi_b\right)} \quad (12)$$

The rolling bearing can be simplified as the mass system with many elastic elements connection, as show in Figure 5. The outer ring of bearing is fixed to the bearing seat and the inner ring is linked to the spindle. The contact deformation between the roller element and the outer ring can be regarded as the spring compression under the radial external force. Therefore, the stiffness of rolling bearing under the radial external load can be expressed as:

$$K = \frac{F}{\delta} \quad (13)$$

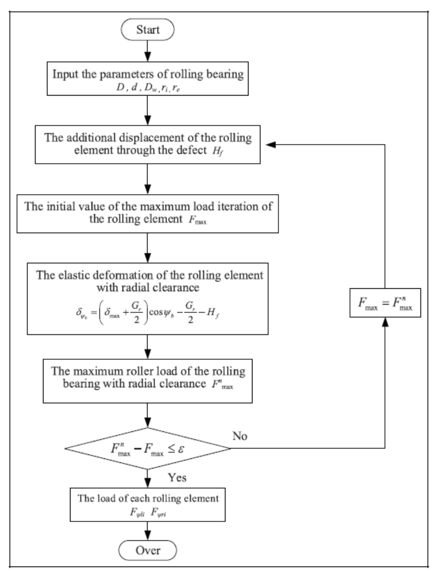

Figure 4. Iterative calculation process.

When $F^n_{\max}-F^{n-1}_{\max}\leqslant\varepsilon$, the iteration finishes, the stiffness of rolling bearing with the outer raceway defect under the radial external load can be expressed as:

$$K = \sum_{li=0}^{nl}\left(\frac{\partial F_{\psi_{li}}}{\partial \delta_{\psi_{li}}}\cdot \cos^2\psi_{li}\right) + \sum_{ri=0}^{nr}\left(\frac{\partial F_{\psi_{ri}}}{\partial \delta_{\psi_{ri}}}\cdot \cos^2\psi_{ri}\right) \quad (14)$$

Where dcli is the contact normal elastic deformation of the rolling element on the left side, li=1, 2, ., nl.

Fcli is the contact normal force of the rolling element on the left side, li=1, 2, ., nl. dcri is the contact normal elastic deformation of the rolling element on the right side, ri=1, 2, ., nr. Fcri is the contact normal force of the rolling element on the right side, ri=1, 2,., nr.

Time-varying stiffness analysis of rolling bearings

Taking the deep groove ball bearing 6206 as an example, the defect length Lb is 2mm, the depth Hb is

1.5mm, and the defect position angle is 0———. The structural parameters and working conditions of the rotor

and bearing are shown in Tables 1 and 2 Based on the rolling bearing stiffness model considering the outer raceway defect, the time-varying

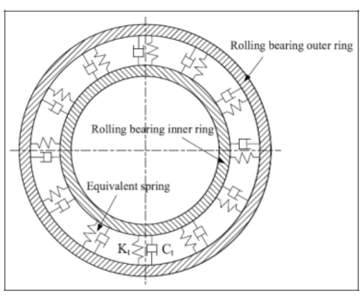

Figure 5. Siffness model of rolling bearing.

stiffness of the defective bearing is calculated. The bear- ing stiffness changing with time shows periodic changes in both horizontal and vertical directions, so it can be fitted as a trigonometric series by Fourier expansion. The stiffness variation curve of the defective bearing in the horizontal and vertical directions is fitted by the MATLAB software. The fitting results of the 8-order Fourier expansions of the bearing stiffness are shown in Figures 6 and 7. The determination coefficients of each order of fitting results (R-squared) are shown in Table 3.

It can be seen from Figure 6 and Table 3 that the horizontal bearing stiffness changing with time is well fitted with the 8-order Fourier series expansion curve. The determination coefficient R-square of the fitting result is 0.9907. From Figure 7 and Table 3, the stiffness in the vertical direction of the bearing changing with time fits well with the 7-order Fourier series expansion curve, and the determination coefficient R-square is 0.9926. The fitting accuracy can both meet the calcula- tion requirements. Therefore, the time-varying stiffness function expressions of the bearing in the horizontal and vertical directions are:

$$K_x(t) = a_{x0} + \sum_{xi=1}^{8}\left(a_{xi}\cos(xi\cdot\omega\cdot t) + b_{xi}\sin(xi\cdot\omega\cdot t)\right) \quad (15)$$

$$K_y(t) = a_{y0} + \sum_{yi=1}^{7}\left(a_{yi}\cos(yi\cdot\omega\cdot t) + b_{yi}\sin(yi\cdot\omega\cdot t)\right) \quad (16)$$

The coefficients of the Fourier expansion in the hori- zontal and vertical directions are shown in Table 4 according to equations (15) and (16).

Table 1. Parameters of deep grove ball bearing 6206.

Parameter	Value	Parameter	Value
Bearing outside diameter D /mm	62	Radius of curvature of inner raceway r_i/mm	4.91
Bearing bore diameter d/mm	30	Radius of curvature of outer raceway r_e/mm	5.00
Bearing width B/mm	16	Inner raceway diameter d_o/mm	36.97
Roller diameter D_w/mm	9.53	Outer raceway diameter D_o/mm	56.03
Pitch diameter D_{pw}/mm	46.5	Sum of inner raceway curvature $\Sigma\rho_i$/mm	0.2701
Quality of bearing m/kg	0.20	Sum of outer raceway curvature $\Sigma\rho_e$/mm	0.1842
Number of rolling elements Z	9	Difference of curvature of inner raceway $F(\rho_i)$/mm	0.9547
Radial load F_r/N	600	Difference of curvature of outer raceway $F(\rho_e)$/mm	0.8915

Table 2. Structure parameters of rotor.

Parameter	Value	Parameter	Value
Length L_{axi}/mm	278	Rotor material	Q235
Quality M_{axi}/kg	1.967	Poisson ratio ν	0.28
Quality and grade of balance G	1	Density ρ/kg m^{-3}	7800
Rotation speed n/r min^{-1}	1500	Modulus of elasticity E/Pa	2.1×10^{11}
Distance between supporting points L/mm	210	/	/

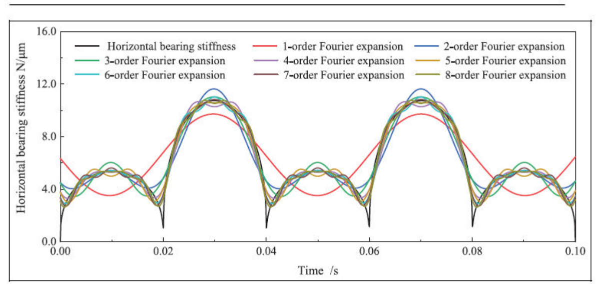

Figure 6. Time-varying stiffness in the horizontal direction.

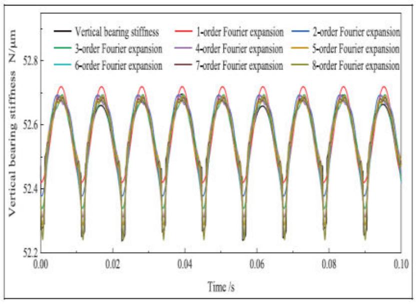

Figure 7. Time-varying stiffness in the vertical direction.

Table 3. Value of R-squared.

Order	1-order	2-order	3-order	4-order	5-order	6-order	7-order	8-order
R-square								
Horizontal direction	0.6462	0.8902	0.9154	0.9524	0.9587	0.9715	0.9801	0.9907
Vertical direction	0.9674	0.9740	0.9744	0.9849	0.9849	0.9849	0.9926	0.9926

Table 4. Fourier expansion coefficients.

Coefficients of horizontal Fourier expansion				Coefficient of vertical Fourier expansion			
Coefficient	Value	Coefficient	Value	Coefficient	Value	Coefficient	Value
a_{x0}	6.616×10^6	/	/	a_{y0}	5.256×10^7	/	/
a_{x1}	-5.891×10^4	b_{x1}	-3.11×10^6	a_{y1}	-1.487×10^5	b_{y1}	-9658
a_{x2}	-1.916×10^6	b_{x2}	5.539×10^4	a_{y2}	-3.757×10^4	b_{y2}	-2.021×10^4
a_{x3}	-3.184×10^4	b_{x3}	-6.184×10^5	a_{y3}	-1.645×10^4	b_{y3}	-2.628×10^4
a_{x4}	-7.474×10^5	b_{x4}	4.014×10^4	a_{y4}	-7665	b_{y4}	-2.772×10^4
a_{x5}	-2.84×10^4	b_{x5}	-3.083×10^5	a_{y5}	176.4	b_{y5}	-2.503×10^4
a_{x6}	-4.373×10^5	b_{x6}	3.742×10^4	a_{y6}	6664	b_{y6}	-1.941×10^4
a_{x7}	-2.409×10^4	b_{x7}	-1.938×10^5	a_{y7}	9799	b_{y7}	-1.256×10^4
a_{x8}	-3.004×10^5	b_{x8}	3.416×10^4	/	/	/	/

Vibration response analysis of rolling bearing rotor system

The time-varying stiffness fitting function of the bearing with outer raceway defects is substituted into equation (1), and the differential equation of motion of the rotor system considering the time-varying stiffness of the bearing and the raceway defects is as follow:

$$M\ddot{x} + C\dot{x} + \left(a_{x0} + \sum_{xi=1}^{8}\left(a_{xi}\cos(xi\cdot\omega_x\cdot t) + b_{xi}\sin(xi\cdot\omega_x\cdot t)\right)\right)x = F_0\sin(\omega\cdot t)$$

$$M\ddot{y} + C\dot{y} + \left(a_{y0} + \sum_{yi=1}^{7}\left(a_{yi}\cos(yi\cdot\omega_y\cdot t) + b_{xi}\sin(yi\cdot\omega_y\cdot t)\right)\right)y = F + F_0\cos(\omega\cdot t) + Mg \tag{17}$$

The differential equation of motion (17) is solved by MATLAB program. When the defect is located at the bottom of the outer raceway of the bearing, its influ- ence on the load distribution, elastic deformation, and contact stress only exists in the vertical direction.31 The time domain of the rolling bearing rotor system with defective outer raceway in the vertical direction are mainly analyzed as shown in Figure 8.

When there is defect in the bearing raceway, the vibration amplitude in the vertical direction of the bearing rotor system increases significantly. However, the vibration amplitude of the rotor system gradually decreases and tends to be periodically stable with the change of time. When the rolling element passes through the defect, the contact stress between the roll- ing element and the bearing raceway, load distribution will change, so the stiffness change period is equal to the rotation time t between the two rolling elements:

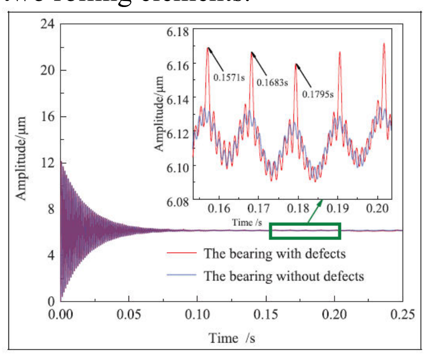

Figure 8. Vertical amplitude of defective bearing rotor system.

$$t = \frac{120D_{pw}}{nZ\left(D_{pw} - D_w\cos\alpha\right)} \tag{18}$$

Where a is the bearing contact angle, and the deep groove ball bearing contact angle is 0°.

According to formula (18), the stiffness change period of bearing 6206 is 0.0112 s. From Figure 6, the rolling element passes through the bearing raceway

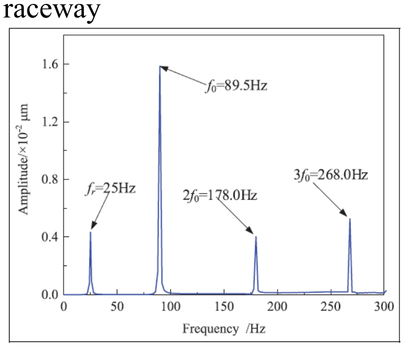

Figure 9. Vertical vibration frequency spectrum of the rolling bearing rotor system with defective raceways.

defect at 0.1571, 0.1683, 0.1795 s, .etc., and the vibra- tion amplitude of the rolling bearing rotor system increases instantaneously. This time interval is consis- tent with the theorical result from formula (18).

On this basis, the vertical vibration spectrum of the raceway bearing rotor system with raceway defects is analyzed by the fast Fourier transform method. The results are shown in Figure 9.

The fault characteristic frequency of rolling bearing outer raceway can be calculated by the following formula32:

$$f_o = \frac{Zf_r}{2}\left(1 - \frac{D_w}{D_{pw}}\cos\alpha\right) \tag{19}$$

Where f_r is the rotor rotation frequency.

The theoretical calculation value of the outer raceway fault characteristic frequency is 89.44 Hz. In Figure 8, the vibration of the rolling bearing rotor system is large at 25, 89.5, 178.0, and 268.0 Hz, which is respectively equal to the rotation frequency of the rotor, the fre- quency of the outer raceway defects of the bearing, dou- ble and triple frequency of outer raceway defect frequency. The corresponding amplitude at the fre- quency of the bearing outer raceway defect frequency is the largest and most prominent.

Vibration test and result analysis of rolling bearing rotor system

Test system

The test system is shown in Figure 10, including vibra- tion test bench, vibration signal acquisition system, and data processing system. The bearings at both ends of the vibration test bench are the tested bearings, which are all deep groove ball bearings 6206 with defects in the outer raceway (as shown in Figure 11). The relevant performance parameters are shown in Table 1. The test bench loads the bearing rotor system through the load- ing bearing. The rotor is drived by the motor through the coupling, and the vibration response is tested by four acceleration sensors symmetrically installed in the 45° direction along the radial direction of the rotor at both ends of the bearing pedestal, as shown in Figure10.The vibration signal of the system is produced by the acceleration sensor, which is amplified by the signal amplifier and then transmitted to the data acquisition card. The output end is connected to the computer and the vibration signal is analyzed and processed by the data processing system. The sampling frequency of vibration signal is 10 kHz, the acceleration sensors are uniaxial piezoelectric sensors. The sensitivity of the

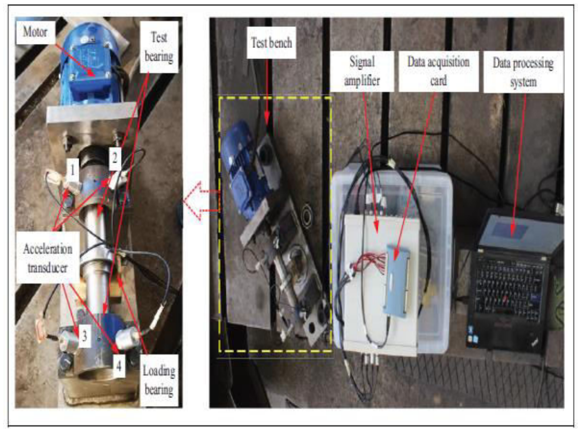

Figure 10. Vibration test bench.

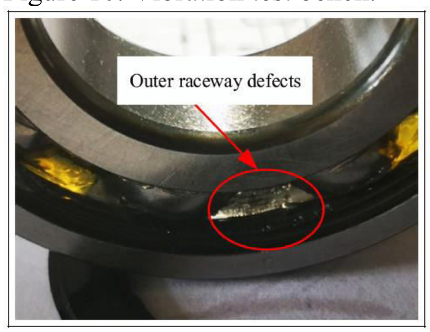

Figure 11. Defective bearing.

sensor is 500 mV g21 and range of data acquisition is from 0.2 to 15 kHz.

Test result analysis

As there is a defect on the outer raceway of the rolling bearing, the bearing rotor system shows obvious abnor- mal vibration. At this time, the vibration signals acquired from the acceleration sensors at the four

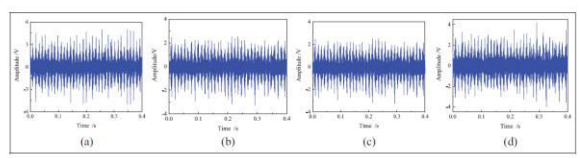

Figure 12. Vibration signal at time domain: (a) monitoring point no. 1, (b) monitoring point no. 2, (c) monitoring point no. 3, and (d) monitoring point no. 4.

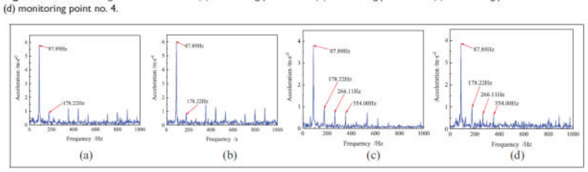

Figure 13. Envelope spectrum of test data: (a) monitoring point no. 1, (b) monitoring point no. 2, (c) monitoring point no. 3, and (d) monitoring point no. 4.

monitoring points of the test bearing at both ends are shown in Figure 12.

The vibration responses at the four points exist obvi- ous vibration shock, especially the monitoring points no. 1 and no. 2 of the front-end test bearing. The envel- ope spectrums of each vibration signal33 are shown in Figure 13

The envelope spectrum of the vibration signal of monitoring points no. 1 and no. 2 at the front bearing shows that the amplitude of the test bearing is the most obvious at the frequency of 87.89 Hz, which is very close to the fault frequency of 89.44 Hz corresponding to theorical calculation and numerical analysis. But the theoretical value is still different from the experimental value. The main reason is that the rolling element is not pure rolling in the test, and the friction loss maybe appear because of the sliding of the rolling element. The lubrication of rolling bearing is not the ideal state in the test, the poor lubrication condition will cause the friction loss. Besides, the size, length, and depth of the defect will also lead to a certain change in the vibration frequency in the test.

At the monitoring points no. 3 and no. 4, the envel- ope spectrum of the vibration signal has the maximum amplitude at 87.89 Hz (as shown in Figure 13), and also has obvious amplitude at its double, triple and quadru- plex frequency.

CONCLUSION

The research successfully demonstrates that radial clearance variation and outer raceway defects significantly influence the vibration signatures of rolling bearing rotor systems. Key findings include a direct correlation between increased radial clearance and higher amplitude vibration responses, as well as the emergence of periodic impact patterns linked to surface defects on the outer raceway. These patterns manifest as distinct peaks in the vibration frequency spectrum, particularly at defect-related frequencies such as the ball pass frequency of the outer race (BPFO).

By applying vibration signature analysis, the study provides diagnostic markers that can help differentiate between clearance-related and defect-induced anomalies. This approach facilitates early detection and classification of bearing faults, enabling more effective condition-based maintenance practices.

In conclusion, understanding the combined effects of radial clearance and raceway defects enhances the precision of bearing health monitoring systems. The findings contribute to improved rotor dynamic analysis, fault tolerance, and reliability engineering in various industrial applications. Future work may explore machine learning integration for automated fault classification based on vibration data.

References

1. Morales-Espejel GE and Wemekamp AW. An engineer- ing drag losses model for rolling bearings. Proc IMechE, Part J: J Engineering Tribology 2023; 237: 415–430.
2. Wu PL, He CL, Chang Z, et al. Theoretical calculation models and measurement of friction torque for rolling bearings: state of the art. J Braz Soc Mech Sci Eng 2022; 44: 24.
3. Chen S, Chen W, Liu J, et al. Development of an aero- static bearing system for roll-to-roll printed electronics. J Micromech Microeng 2018; 28: 065002.
4. Yang R, Zhang Z and Chen Y. Analysis of vibration sig- nals for a ball bearing-rotor system with raceway local defects and rotor eccentricity. Mech Mach Theory 2022; 169: 14.
5. Savic B, Urosevic V, Ivkovic N, et al. Implementation of a non-linear regression model in rolling bearing diagnos- tics. Tehnicki Vjesn 2022; 29: 314–321.
6. Hu G, Chen Y, Cui L, et al. Investigation on modeling and formation mechanism of dynamic rotational error for spindle-rolling bearing system. Appl Sci 2020; 10: 5753.
7. Stribeck R. Ball bearings for various loads. Trans ASME 1907; 29: 420–426.
8. Elastic PH. Elastic Spielschwingungen Konstant Walzl- ger. Werkstatt und Betrieb 1950; 3: 354–358.
9. Larizza F, Moazen-Ahmadi A, Howard CQ, et al. The importance of bearing stiffness and load when estimating the size of a defect in a rolling element bearing. Struct Health Monit 2019; 18: 1527–1542.
10. Nakhatakyan FG, Puzakina AK and Nakhatakyan DF. The importance of bearing stiffness and load when esti- mating the size of a defect in a rolling element bearing. Struct Health Monit 2022; 49(47): 591–603.
11. Zhang XN, Han QK, Peng ZK, et al. Stability analysis of a rotor-bearing system with time-varying bearing stiff- ness due to finite number of balls and unbalanced force. J Sound Vibr 2013; 332: 6768–6784.

12. Li XP, Chen RZ, Shang DY, et al. Dynamic response of maneuvering flight friction rotor with variable stiffness bearing. J Harbin Inst Technol 2020; 52: 1–7.
13. Cheng H, Zhang Y, Lu W, et al. Mechanical characteris- tics and nonlinear dynamic response analysis of rotor- bearing-coupling system. Appl Math Model 2021; 93: 708–727.
14. Petersen D, Howard C and Prime Z. Varying stiffness and load distributions in defective ball bearings: analyti- cal formulation and application to defect size estimation. J Sound Vib 2015; 337: 284–300.
15. Chen RL, Zhao SD, Zhang MH, et al. Time-varying stiff- ness model and load-bearing characteristics analysis of angular contact ball bearings. Mach Des Res 2022; 38: 114–119.
16. Cao H, Li Y, He Z, et al. Time varying bearing stiffness and vibration response analysis of high speed rolling bearing-rotor systems. J Mech Eng 2014; 50: 73–81.
17. Liu Y and Zhang Y. A research on the time-varying stiff- ness of the ball bearing considering the time-varying num- ber of laden balls and load distribution. Proc IMechE, Part C: J Mechanical Engineering Science 2019; 233: 4381–4396.
18. Cheng H, Zhang Y, Lu W, et al. Research on time- varying stiffness of bearing based on local defect and varying compliance coupling. Measurement 2019; 143: 155–179.
19. Petersen D, Howard C, Sawalhi N, et al. Analysis of bearing stiffness variations, contact forces and vibrations in radially loaded double row rolling element bearings with raceway defects. Mech Syst Signal Process 2015; 50–51: 139–160.
20. Cui L, Zhang Y, Zhang F, et al. Vibration response mechanism of faulty outer race rolling element bearings for quantitative analysis. J Sound Vib 2016; 364: 67–76.